Energy loss of hydrogen projectiles in gases

A. Schiefermüller, R. Golser, R. Stohl, and D. Semrad
Institut für Experimentalphysik, Johannes-Kepler-Universität, A-4040 Linz, Austria
(Received 1 March 1993)

The stopping cross sections of H_2, D_2, He, and Ne for hydrogen projectiles in the energy range 3–20 keV per nucleon have been measured by time of flight. We compare our experimental result to the sum of the individual contributions due to excitation and ionization of the target and of the projectile, respectively, and due to charge exchange, using published cross-section data. Satisfactory agreement is found only for the He target and only at moderate projectile velocities, whereas for H_2 and D_2 the calculated values are about 30% too low. A Monte Carlo program allows us to simulate the measured time-of-flight spectra and to explain minor trends in the experimental data: for increased Ne gas pressure, an increased specific energy loss has been found that can be traced to different regions of impact parameters selected in our transmission geometry. This also explains, in part, the increased specific energy loss for deuterons compared to protons of equal velocity that is most evident for Ne. In contrast, a decrease of the specific energy loss with increasing pressure for He may be explained by impurities in the target gas. If we correct for the effect of impurities, the stopping cross section of He at 4 keV per nucleon is slightly smaller (0.60×10^{-15} eV cm^2) than published earlier (0.72×10^{-15} eV cm^2) and depends on the 3.8th power of projectile velocity.

PACS number(s): 34.50.Bw

I. INTRODUCTION

The various collisions processes which take place when hydrogen projectiles of several keV penetrate gaseous targets have been studied extensively in the past. A huge amount of cross-section data [1–3] is available for collisions where the target or the projectile is excited or ionized or where an electron is transferred from the target to the projectile. As the energy necessary for all processes comes from the projectile's kinetic energy, a measurement of the stopping cross section provides a consistency check for the individual cross sections. So atomic collision physics can profit from high-quality stopping measurements. Furthermore, these stopping data are also of considerable importance to radiotherapy as the energy deposited by heavy projectiles in tissue is often deduced from the energy loss in equivalent *gases*.

Recently, we have developed a time-of-flight (TOF) apparatus to measure the stopping cross section ϵ of gases for light ions in the energy range from 3 to 20 keV per nucleon. The quantity ϵ is defined by

$$\epsilon=-\frac{1}{N}\frac{dE_1}{dx}=\sum_i T_i\sigma_i(E_1)\ , \tag{1}$$

where E_1 is the kinetic energy of the projectile, N is the number density of target atoms or molecules, and x is the path length measured along the projectile's trajectory; T_i denotes the projectile's energy loss associated with a particular collision process i, whose cross section is given by σ_i. The definition of ϵ as a sum over all possible inelastic processes implies that a stopping cross-section measurement must not be impact-parameter selective but should, in principle, accept *all* projectiles (i.e., accept projectiles within 4π solid angle). We have shown [4] that the customary assumption that ϵ is exactly proportional to the first power of projectile velocity v_1 at velocities below the Bohr velocity v_0 does not hold in general: for protons at 4 keV in helium gas a dependence on at least the third power of v_1 has been observed. From the interpretation of this experiment we also concluded that in a gas mixture a large deviation from Bragg's rule, which assumes additivity of the individual stopping cross sections, should occur [5].

In this paper we would like to thoroughly discuss the stopping process of hydrogen projectiles in the atomic gases helium and neon, and (to a lesser extent) in molecular hydrogen gas (H_2 and D_2). We compare the measured TOF spectra to a Monte Carlo (MC) calculation where we use refined cross sections for the inelastic processes mentioned above and assume a simple impact-parameter dependence of these processes. From the MC simulation we also get the contribution of elastic collisions, which allows us to extract the electronic energy loss from the measured total (electronic plus nuclear) stopping. In Sec. II we present a short description of the experimental setup and of the evaluation procedure. In Sec. III the assumptions entering our MC code are given, and in Sec. IV we discuss the results for the gases Ne, He, H_2, and D_2.

II. EXPERIMENTAL DETAILS

A. Measurement of ϵ by time of flight

Projectiles—protons or deuterons—are produced in a duoplasmatron ion source and are accelerated by an immersion lens. The voltage across the lens may be varied from 6 to 20 kV and has been shown to correspond to the kinetic energy E_0 of the ion beam within 20 V. After col-

limation by B_1-B_2 (cf. Fig. 1) the beam is momentum analyzed by the 60° deflection magnet M. The region between B_4 and B_5 is our target gas cell, 210 cm in length. A differentially pumped aperture B_3-B_4 (diameter 0.2 cm) forms the target entrance over which the ion beam is swept electronically by two pairs of deflection plates; a thin carbon foil (150 Å) covers the gas-cell exit hole B_5 of about 0.4 cm diameter. Fifty circular apertures arranged along the flight path absorb projectiles that have been scattered more than 3 cm off the chamber axis. The target pressure may be chosen in the range from 0.01 to 0.15 mbar. It is measured by a capacitive manometer and is regulated within 1×10^{-4} mbar.

The TOF start pulse is derived from the deflection voltage on the plates, and the stop pulse is provided by a multichannel plate (MCP) mounted 3.1 cm downstream of the exit foil at B_5. Both pulses are processed by high-speed electronics, and after time-to-amplitude conversion the TOF spectrum is acquired by a multichannel analyzer (MCA). A digital time delay allows us to calibrate the MCA's time scale.

The mean energy loss is derived from the difference between TOF spectra with the gas cell evacuated ($<1\times10^{-5}$ mbar) and with the cell filled. First the TOF spectrum is measured without target gas. After a series of measurements at constant beam energy E_0 with target gas at different pressures, spectra without gas are taken again; the very small difference observed for the spectra without gas (of the order of 1 ns) is assumed to vary linearly in time; it is most likely due to a small drift of E_0 and due to an increased energy loss in the exit foil after having been exposed to gas.

Our experimental errors, which are to be understood as one standard deviation, depend on the projectile-target combination and on the beam energy. The total error due to the contributions described below amounts to about 11–14% at low velocities and to about 7% at high velocities.

To keep a reasonable counting rate in spite of losses due to multiple scattering, the maximum gas pressure is limited, especially at low energies. The error of the target areal mass density (that includes the error of the target temperature) varies between 2% at high energies and 5% at low energies. Since in our energy range ϵ decreases with decreasing projectile velocity, the measured differences in TOF decrease as well. Errors of the TOF measurement are due to uncertainties in the determination of the first moment of the time spectra, due to the drift of the beam energy, and due to changes of the time shift caused by a gas load on the exit foil; they add to 5–7 % at 4 keV per nucleon (depending on gas species and on gas pressure) and to 2% at 20 keV per nucleon. All individual errors mentioned so far are considered as random errors and have been summed geometrically. Systematic errors are due to uncertainties in the effective length of the flight path (2%), due to the manometer accuracy (2%), and due to time calibration (0.5%); these errors have been added algebraically.

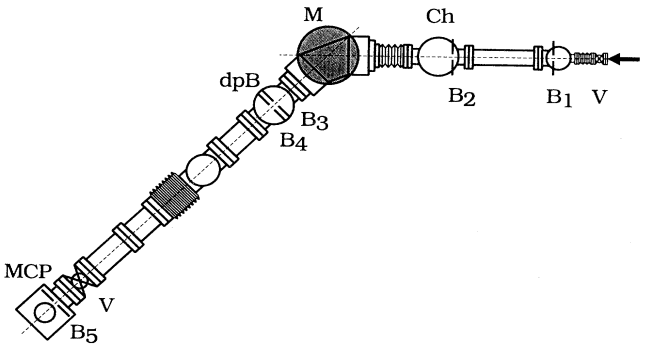

FIG. 1. Layout of the TOF experiment. The abbreviations are Ch, deflection plates for beam chopper; M, 60° bending magnet; dpB, differentially pumped baffle B_3-B_4; MCP, multichannel plate; B_i, baffle; V, valve. The target gas cell is the region from B_4 to B_5, 210 cm in length; B_5 is covered by a 150-Å carbon foil.

B. Conversion of time spectra to energy spectra

When evaluating the measurements we have to keep in mind that the target gas cell is a considerable part of the total flight path. Therefore there is no unique correspondence between the energy lost by a projectile and its TOF, as this quantity also depends on the position where the individual energy-loss processes take place [6]. Whereas the width of the energy distribution is entirely due to energy-loss straggling, an additional contribution to the width of the TOF distribution comes from fluctuations in the positions [6]; this "position straggling" might lead to a bias in the calculated first moment of the energy-loss distribution. Therefore we have solved numerically the Boltzmann equation in the energy-time domain that governs the one-dimensional transport of projectiles along the chamber axis. We have shown [6] that the mean energy loss may be obtained from the mean TOF with an accuracy of better than 0.1% by integrating the equation of motion in the continuous-slowing-down approximation (CSDA). Within a limited energy range the dependence of the stopping cross section on projectile velocity may be expressed by a power law, $\epsilon=\alpha v_1^{\beta}$; the proportionality factor α and the exponent β have to be adjusted iteratively. The "stopping power" $N\epsilon$ is really a decelerating force, so in the CSDA it may be expressed in terms of the flight path x and the TOF t:

$$m\frac{d^2x}{dt^2}=-N\alpha\left[\frac{dx}{dt}\right]^{\beta}. \tag{2}$$

At the target entrance opening, $x=0$, $t=0$. At $x=L$, the length of the gas cell, and with t equal to the mean of the measured TOF distribution, the integral of Eq. (2) yields a very good estimate for ϵ, given by α and β.

III. MONTE CARLO SIMULATION

To go beyond the CSDA and also beyond the one-dimensional Boltzmann equation mentioned above, a Monte Carlo simulation seems appropriate. It allows us not only to study the influence of projectile scattering upon the energy loss measured with our experimental

geometry, but offers additional advantages: charge-state preequilibrium effects due to the transient region at the target entrance may be simulated, and the target composition can be varied, so the influence of residual gas on energy loss can be investigated.

The MC program helps also to extrapolate the energy loss measured with our angle-restricted transmission geometry to the "correct" 4π geometry. Since the transport of projectiles is simulated both in the energy domain and in the time domain, the MC results may be directly compared to the measured TOF spectra. We find in general that when using published cross-section data for the inelastic processes, the simulation differs considerably from experiment. We wish to mention already at this point that in order to match the first moments of the simulated and of the measured TOF spectra we multiply the relevant cross sections from the literature by a common factor. By inserting these "corrected" cross sections into Eq. (1), we get the "true" ϵ. The details follow in Sec. IV.

A. Impact-parameter-dependent energy loss

Projectiles that have suffered a scattering process with a small impact parameter have on the average lost comparatively large amounts of energy to the nucleus and to the electrons. In our transmission experiment these projectiles are scattered out of the direction to the detector with high probability but they may get rescattered into the detector by subsequent collisions. Hence, for a fixed experimental geometry and for a given projectile-target combination at a given energy, the probability of a projectile being detected depends on target pressure p and thus an influence of p on the measured *specific* mean energy loss is to be expected. (We define the specific mean energy loss as the mean energy loss derived from experiment divided by the target areal density; we wish to distinguish here between specific mean energy loss and stopping cross section which must not depend on experimental conditions.) The influence of impact-parameter-dependent (IPD) energy loss can be clearly seen in our results for Ne discussed in Sec. IV; there we will also show that the observed effect can only be explained by IPD electronic stopping (since IPD nuclear stopping is much too small).

The concept of IPD energy loss has been postulated after careful measurements of ϵ in solids at MeV proton energies [7]. It manifests itself primarily as an increased electronic energy loss for projectiles scattered off the incoming direction [8,9]. If only projectiles are detected that leave the target in the direction of the incoming beam, a *specific* energy loss increasing slightly with increasing target thickness [10] should be observed: for the thicker targets there is an enhanced probability that projectiles scattered by comparatively large angles are rescattered into the detector. However, one has to bear in mind that target thickness inhomogeneity establishes an apparently similar correlation between exit angle and energy loss: due to multiple scattering the thinner parts of the target (with relatively small energy loss) contribute excessively to the measurement at zero degree; if divided by the *mean* target thickness this results in too small values of specific energy loss. The relative thickness variation usually becomes smaller for thicker targets, thus causing the specific energy loss to increase.

We have seen that our transmission experiment is influenced by impact-parameter selection. However, since we do not work in the single scattering regime, we cannot investigate IPD energy loss in detail. Fortunately, for purposes of our stopping experiment, we need not investigate in detail: with gaseous targets at low pressures, IPD energy loss is obscured by an effect which we call "intrinsic target inhomogeneity." From adiabatic arguments it follows that there is a maximum impact parameter $b_{\max}$ up to which energy-loss processes are possible; $b_{\max}$ is much larger than impact parameters leading to noticeable scattering angles, but in dilute gases $b_{\max}$ is appreciably smaller than the mean distance $\bar{d}$ between gas molecules. Hence projectiles normally pass a thin layer of target gas without any interaction. Consider the following example: 10-keV deuterons traversing the length $L=210$ cm of Ne gas at $p=0.02$ mbar and assume $b_{\max}=2.4a_0$; ($L=4.0\times10^{10}a_0$, where a_0 denotes the Bohr radius; p corresponds to an atomic density $N=7.3\times10^{-11}a_0^{-3}$; $\bar{d}=2.4\times10^{3}a_0$). The mean number of interactions for one projectile is about 50; assuming a Poissonian distribution, this number will have a standard deviation of 14%. We called this effect due to collision statistics "intrinsic target inhomogeneity." (The mean number of inelastic collisions might even be lower, since the reaction probability needs not to be 1 within $b_{\max}$, as may be seen from the mean total energy loss of 180 eV and the average energy loss per process of about 10 eV.)

Intrinsic target inhomogeneity is correctly accounted for in our MC program by assuming the free flight paths to follow an exponential distribution. As mentioned before, the intrinsic target inhomogeneity tends to conceal the effect of IPD energy loss. Therefore our stopping experiment is rather insensitive to details of the functional dependence of energy transfer cross sections on impact parameter and the simple model introduced in Sec. III C will suffice to reproduce the measured spectra.

B. Nuclear stopping

To find the dependence of the scattering angle θ on the impact parameter b for a *screened* Coulomb potential, we have calculated the scattering integral numerically with impact parameters ranging from $0.01a_0$ to $3a_0$, and for energies from 3 to 50 keV. The scattering potential has been calculated from the electron wave functions by Clementi and Roetti [12] and has been corrected for the influence of the projectile by reducing the screening length [13]; dynamic aspects of the projectile-target interaction were neglected. At a given impact parameter, $\tan(\theta/2)$ for the screened potential in the laboratory system has been divided by the corresponding value for the pure Coulomb potential $\tan(\theta_C/2)$; this ratio has been fitted by suitable analytical functions that allow us to rapidly calculate θ with an accuracy of better than 0.1° in the whole range of interest.

The elastic energy transfer is derived from the scatter-

ing angle assuming the target to be at rest. Integration over all impact parameters yields the nuclear stopping cross section ϵ_{nucl}. In Fig. 2 we show this quantity for deuterons incident onto deuterium, helium, and neon. Also plotted are the results from the universal function given by Lindhard, Nielsen, and Scharff [14], which is based on the Thomas-Fermi model of the atom.

C. Electronic stopping

The electronic stopping cross section is given by the sum of the cross sections σ_i for excitation and ionization and for charge transfer, multiplied by the corresponding mean energy transfer T_i [cf. Eq. (1)]. The impact-parameter dependence of electronic energy loss ΔE_{el} is due to the impact-parameter dependence of the underlying inelastic collision processes. At high velocities, calculations show that within certain limits the energy loss can be taken proportional to the areal density of electrons along the projectile's trajectory through the target atom [15]. This results in a smooth monotonic dependence of ΔE_{el} on b, which has been found also by other calculations [16,17]. At low velocities, however, the harmonic-oscillator model [18] already gives an oscillatory behavior for $\Delta E_{\text{el}}(b)$; for certain transitions in real atoms this trend is even more pronounced [19]. Unfortunately, the impact-parameter dependences of inelastic cross sections for the targets considered here are not all known. Fortunately, even a very simple model for IPD electronic energy loss will suffice (see above).

We may confine our considerations to collisions with impact parameters smaller than a certain b^*, which give rise to relatively large scattering angles and hence to an increased probability that the projectile will miss the detector. This may be seen from Fig. 3, where the result of a MC calculation for 8-keV deuterons in neon is displayed. Here we show the *relative* probability for a projectile that has entered the detector to have been affected by a certain impact parameter b; the actual number of encounters with impact parameter b depends on

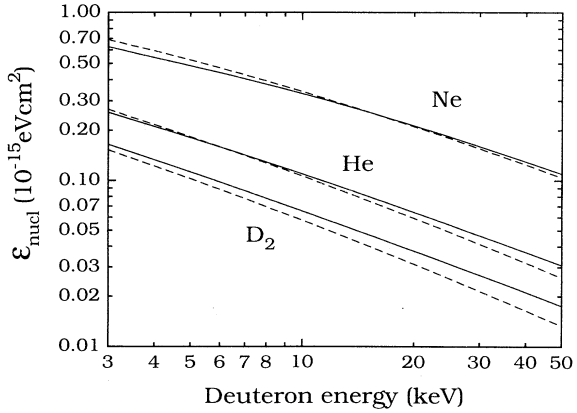

FIG. 2. The nuclear stopping cross section ϵ_{nucl} of three gases for incident deuterons as calculated from a numerical solution of the scattering integral. The broken lines give the result of Lindhard, Nielsen, and Scharff [14].

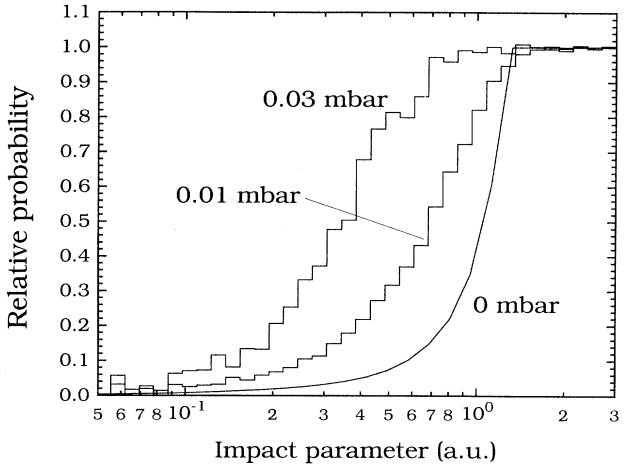

FIG. 3. The relative probability for an 8-keV deuteron that enters our detector to have been affected by a certain impact parameter, after transversing Ne gas at a given pressure (see text).

statistics and is *not* considered here. For the curve labeled "0 mbar" we assume that exactly one scattering event has happened; if b is about equal to a_0 or greater, the scattering angle is small and the projectile will be registered regardless of the position of the collision along the flight path; if b is less than a_0, detection probability depends on the distance of the scattering event from the exit baffle. With increasing pressure it is more likely that a projectile once scattered out of acceptance will be rescattered and detected. This may be compared to Fig. 3 of Ref. [20] (200-keV protons traversing a 180-Å gold foil): whereas we consider projectiles at certain *distances* from the axis, Ref. [20] deals with projectiles at different *angles,* but both figures show the same tendency due to the close relation between the lateral and angular multiple scattering distribution [21,22].

To describe ionization of the target and stripping of the projectile, we represent the target atom by circular discs of area $\sigma_j = P_j \pi b_j^2$, where P_j is the respective reaction probability which is taken constant up to b_j. A judicious choice of the parameters P_j and b_j permits fine tuning of the pressure dependence. Cross sections for excitation of the target and of the projectile, respectively, and of electron capture are arranged as nonoverlapping rings outside of b^*; obviously, the detailed shape of these areas has no influence on the mean energy loss if a large number of projectiles is involved or if each projectile undergoes a large number of collisions; therefore we assume unit reaction probabilities. A graphical representation of our choices is given in Sec. IV.

D. MC calculation

As the program allows us to simulate the passage through a mixture of gases, the next collision partner is determined by a first random number according to the target composition weighted by the respective cross sections. The mean free path between two subsequent collisions follows from the maximum impact parameter

b_{max}, up to which elastic or inelastic processes are possible. b_{max} depends on the target species and on the projectile's energy and charge state (b_{max} is always less than $2.7a_0$ in our cases). The actual path length is exponentially distributed and is determined by a second random number. Two further random numbers give the impact parameter b and the azimuth ϕ of this scattering event. Nuclear and electronic energy losses are both determined by b as described before.

Usually, the projectiles enter the target as protons or deuterons, but incident neutral projectiles may be simulated, too. The charge state inside the target will be +1 or 0 and is determined by the history of collision events which led to capture or loss of electrons. (Negatively charged projectiles have been included in the case of H_2 and D_2 but may be safely ignored for He and Ne.) The calculation is stopped if a projectile impinges on the exit foil or if it leaves the region bounded by the antiscattering baffles. Energy-loss straggling in the foil, which increases the TOF straggling on the flight path to the detector, is taken into account by adding a Gaussian term. The width of this term has been obtained from measurements with and without the exit foil.

IV. RESULTS

A. Preequilibrium stopping

In general we found by the MC simulation that when we use bare projectiles, we may safely neglect any difference of energy loss before and after charge-state equilibrium is reached. The mean charge state is predominantly determined by the cross section for electron capture, which is more sensitive to the projectile-target combination than the stripping cross section. In H_2 and D_2, the hydrogen projectiles are almost all neutral due to the large capture cross section, but since here the relaxation length is short, equilibrium is soon established. The opposite applies to He and in part to Ne, where the small capture cross section leads to a projectile ionized for most of the time: therefore, for incident protons or deuterons, the large relaxation length has little influence, since the equilibrium charge state is almost equal to the charge state of the incoming particle. If one would use neutral projectiles, this condition would not be met; for this case, the simulation gives a large effect of preequilibrium stopping.

B. Neon

In Fig. 4 we show the raw data of the specific mean energy loss measured with hydrogen projectiles in Ne. Each single measurement is represented by a short line starting at the energy E_0 of the incident ion and ending at the energy of the projectile just in front of the exit foil; the length of a line thus indicates the energy lost in the target gas and is therefore proportional to the target pressure p. Data points below 10 keV per nucleon have been taken with deuterons, those above 10 keV with protons, and those at $E_0 = 10$ keV per nucleon with both isotopes. We find a definite dependence of the measured specific energy loss on p which is due to IPD energy loss.

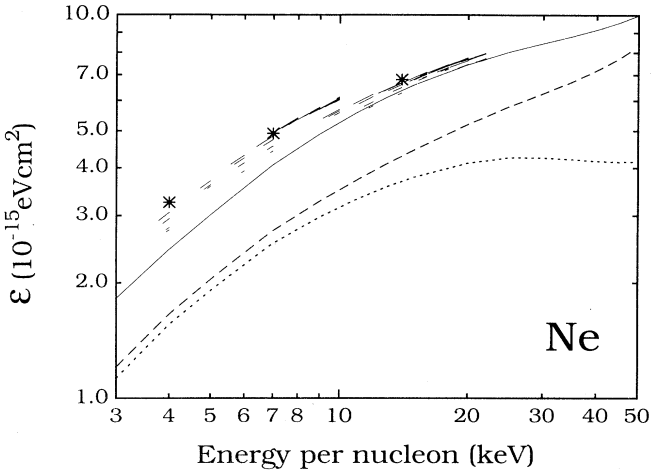

FIG. 4. Specific mean energy loss of protons and deuterons in Ne. The short lines indicate the range of the projectile energy in individual measurements. The asterisks mark the calculated "true" stopping cross sections. The three curves give in a *cumulative* manner the contributions to ϵ from three groups, calculated with the (uncorrected) data from the literature: the dotted curve shows only the contribution of charge-changing processes, the dashed curve corresponds to charge-changing processes plus stopping processes at fixed projectile charge state +1, and the full curve corresponds to all inelastic processes, i.e., it includes also the contribution of energy-loss processes at fixed projectile charge state 0.

Figures 5(a) and 5(b) are the graphical representations of the models used in the MC simulation for 4-keV protons and hydrogen atoms, respectively. The impact-parameter scale is quadratic; this makes the plotted areas proportional to the cross sections. All cross sections from the literature were multiplied by a factor 1.33 (see below). The model covers all processes that make important contributions to energy loss and also those of minor importance if data are available; no attempt was made to estimate lacking values. The charge-changing cross sections are from Ref. [23]. For the neutral projectile, only excitation to the L and M shells [24] is taken into account, as higher excitation levels will be less populated; the long-living $2s$ state is assumed to be ionized by subsequent collisions. Concerning Ne excitation, we only found cross sections for excitation to the $2p^5 3s$ state, and only for protons [25]. Cross sections for ionization of Ne by protons have been derived from the semiempirical fit functions for the differential cross sections tabulated in Ref. [26]; ionization cross sections for Ne by neutral hydrogen projectiles are from Ref. [27].

The energy transfers associated with the processes given in Fig. 5(a) have been calculated as follows. The energy required for Ne ionization from the $2p$ state is 21.6 eV; 7.2 eV have been added for the mean kinetic energy of the released electron [26] (here we take the same value for incident hydrogen atoms as for protons; it is derived from the differential cross sections by integration). Projectile ionization requires 13.6 eV plus the mean kinetic energy of the ionized electron in the laboratory system, 5.6 eV; this value is based upon data from pro-

tons incident onto H_2 [28] assuming the velocity distribution of the emitted electrons in the frame of the projectile to be isotropic. For higher energies the electrons are emitted with larger velocities but their distribution becomes peaked in the backward direction [26]; this is taken into account by keeping the value of 5.6 eV for all energies (Ref. [26] deals with target ionization, we apply their result to projectile ionization). For the processes in Fig. 5(b), the energy transfers were obtained in the following way: ionization of target $2s$ electrons requires 48 eV plus the mean kinetic energy of the electron, 12.2 eV [26]; ionization of target $2p$ electrons costs 21.6 eV plus 7.2 eV for the electron's mean kinetic energy. Electron capture by the projectile requires 8 eV due to the different binding energies of target and projectile, plus 2.2 eV for the electron changing to the projectile's frame of reference.

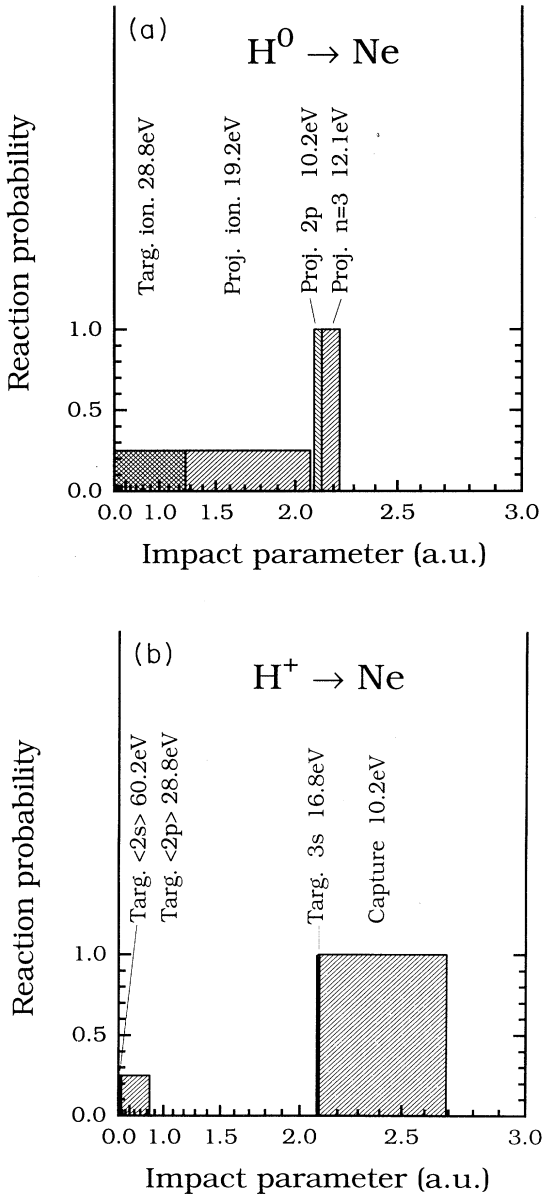

FIG. 5. Our model for the Ne atom with respect to the electronic energy loss of 8-keV hydrogen atoms (a) and protons (b). The abbreviations are Targ., target; Proj., projectile; ion., ionization from ground state; $\langle 2s \rangle$, ionization from $2s$; $\langle 2p \rangle$, ionization from $2p$; $2p$, excitation to $2p$; $n=2$, $n=3$, excitation to the $n=2$ or $n=3$ shell, respectively. The energy values given correspond to the values T_i [Eq. (1)]; see also the text.

In Fig. 6 we have plotted the measured TOF spectrum and the result of the simulation using our atomic model; it applies to deuterons with 4 keV per nucleon in Ne at a pressure of 0.02 mbar. As mentioned before, the first moments of the two distributions have been matched by multiplying the relevant cross sections from the literature by the factor 1.33. The shapes of the spectra agree extremely well, even up to high TOF values. In Table I we compare the measured and the calculated specific energy loss as a function of target pressure; the trend found in our measurements is well reproduced. The MC simulation allows us to separate the contributions from nuclear and electronic collisions; obviously nuclear energy losses are too small to explain the pressure dependence. Also given are the nuclear stopping cross section taken from Fig. 2 and the "true" electronic stopping cross section ϵ as defined by Eq. (1), i.e., obtained by summing all energy losses multiplied by the respective (corrected) cross sections. In Fig. 4 the "true" ϵ values are plotted by asterisks at three energies. We cannot, by our simulation, fully explain the difference between data taken with protons and with deuterons, respectively, at 10 keV per nucleon; the difference might be due to the Coulomb effect [29].

The curves in Fig. 4 show the (uncorrected) individual contributions in a *cumulative* manner: the dotted curve gives only the contribution of processes that change the projectile's charge, the dashed curve shows stopping of the bare projectile nucleus plus the charge-changing contribution, and the full curve corresponds to all processes

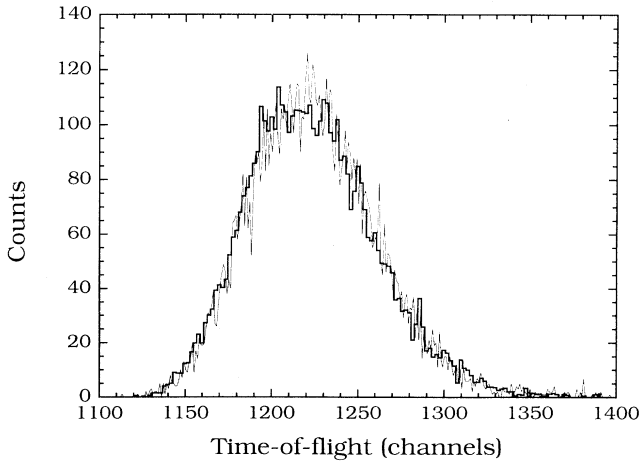

FIG. 6. Comparison of the measured (light line) and the simulated (heavy line) TOF spectrum of 8-keV deuterons through 0.02-mbar Ne. The spectrum without gas (not shown) peaks at channel 1102.8, with a full width at half maximum of ten channels. One channel corresponds to 0.189 nsec.

TABLE I. Dependence of specific mean energy loss of deuterons in Ne on gas pressure p as measured and as obtained from MC simulation ($\Delta E/N\Delta x$ in units of 10^{-15} eV cm^2). The simulation allows one to separate the contributions from electronic and nuclear energy losses. The underlined values are the nuclear stopping cross section taken from Fig. 2 and the "true" electronic stopping cross sections (which would be measured in a 4π geometry), calculated from refined data on the individual collision processes.

Deuteron energy (kev)	p (mbar)	$\Delta E/N\Delta x$ (measured)	$\Delta E/N\Delta x$ (simulated electronic stopping)	$\Delta E/N\Delta x$ (simulated nuclear stopping)
8	0.01	2.79	2.78	0.02
	0.02	2.95	2.94	0.04
	0.03	3.06	3.04	0.05
			3.18	0.38
14	0.01	4.43	4.45	
	0.02	4.56	4.60	
	0.03	4.75	4.75	
			4.92	0.27

contributing to ϵ [Eq. (1)], i.e., charge changing plus the partial stopping contributions from the bare and the neutral projectile, respectively. Since the data from the literature have not been corrected for calculating the curves, we see that the full curve is smaller than the "true" ϵ by a factor of 1.33 at 4 keV, by 1.21 at 7 keV, and by 1.07 at 14 keV.

We observe for Ne a significant deviation from velocity proportional stopping: writing the v_1 dependence of ϵ in the form $\epsilon \propto v_1^{\beta}$, we find $\beta=0.83$ at 20 keV (per nucleon), $\beta=1.2$ at 10 keV, $\beta=1.4$ at 7 keV, and $\beta=1.7$ at 4 keV.

C. Helium

Figure 7 shows the result of our measurements with hydrogen isotopes penetrating He gas. Here, a much larger deviation from velocity proportionality is evident. Looking for details, we find the specific energy loss to decrease with increasing He pressure, predominantly at low velocities, where ϵ is small. This behavior is contrary to that of Ne, and may be explained by assuming an admixture of small amounts of impurities (most likely water) to the target gas. The main effect of the impurity gas is to neutralize the projectiles more effectively than He and therefore to strongly enhance charge-changing cycles; this leads to a large deviation from Bragg's rule [5]. In the simulation we use hydrogen gas instead of water, since both have comparable cross sections for electron transfer to the projectile, and since the necessary data are easily available (see next section). A constant residual H_2 pressure of 1.8×10^{-4} mbar in the MC simulation gives the best agreement with the observed pressure dependence; this is roughly the equilibrium pressure when the flight tube is pumped only via the small entrance aperture and no He is admitted.

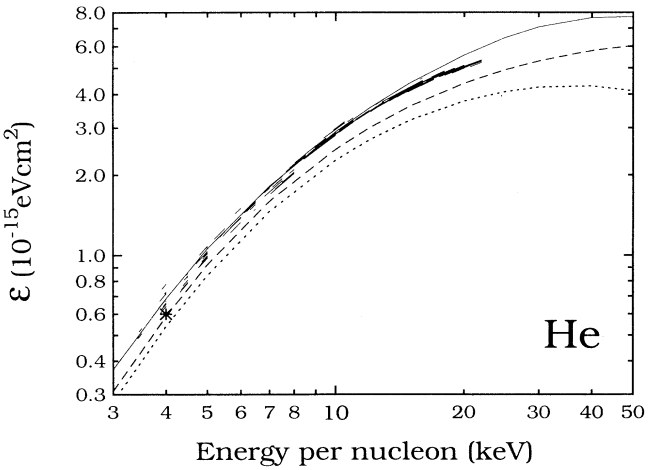

FIG. 7. Specific mean energy loss of protons and deuterons in He. For details, see caption of Fig. 4.

In the following we cite the measured and the simulated specific energy loss of 8-keV deuterons in our He target (the values are in units of 10^{-15} eV cm^2): at 0.01 mbar we have measured 0.728, the simulation yields 0.73, at 0.08 mbar the experiment yields 0.643 and the simulation yields 0.65. Corrected for impurities, the value ϵ at 4 keV per nucleon is now 0.60×10^{-15} eV cm^2, instead of the value 0.72×10^{-15} eV cm^2 given in Ref. [4] (part of this reduction comes from the remeasured energy loss in the exit foil). The corrected values for the exponent of the velocity dependence are $\beta=3.8$ at 4 keV (instead of 3.34 [4]), and $\beta=2.4$ (2.23, [4]) at 10 keV.

In Figs. 8(a) and 8(b) we show the cross sections used for the MC simulation of 8-keV deuterons in He. The values from the literature have been multiplied by 0.85 to make the simulation agree with the measurement: cross sections for charge changing, for excitation of the projectile, and for excitation of He to the L and M shells by protons are taken from Ref. [3]. As no data were found for excitation to the L shell by neutral projectiles, an n^{-3} law [1] was assumed to scale the cross sections from excitation to the M shell [3] (n denotes the main quantum number). Ionization cross sections for He are from Ref. [26].

The most conspicuous differences compared to Ne are the small cross sections for the inelastic processes of protons in He, especially that for electron capture [Fig. 8(b)

compared to Fig. 5(b)]. This is the reason for the small specific energy loss and the strong deviation of ϵ from a v_1-proportional dependence at low velocities: The velocity is too small for efficient excitation or ionization of the He atom by the bare proton [29] via direct Coulomb interaction. So stopping is dominated by capture and loss of electrons by the projectile (cf. Fig. 7); however, these charge-changing collisions are rather inefficient on an absolute scale since the neutralization cross section of protons in pure He is rather small due to the large mismatch of the binding energies.

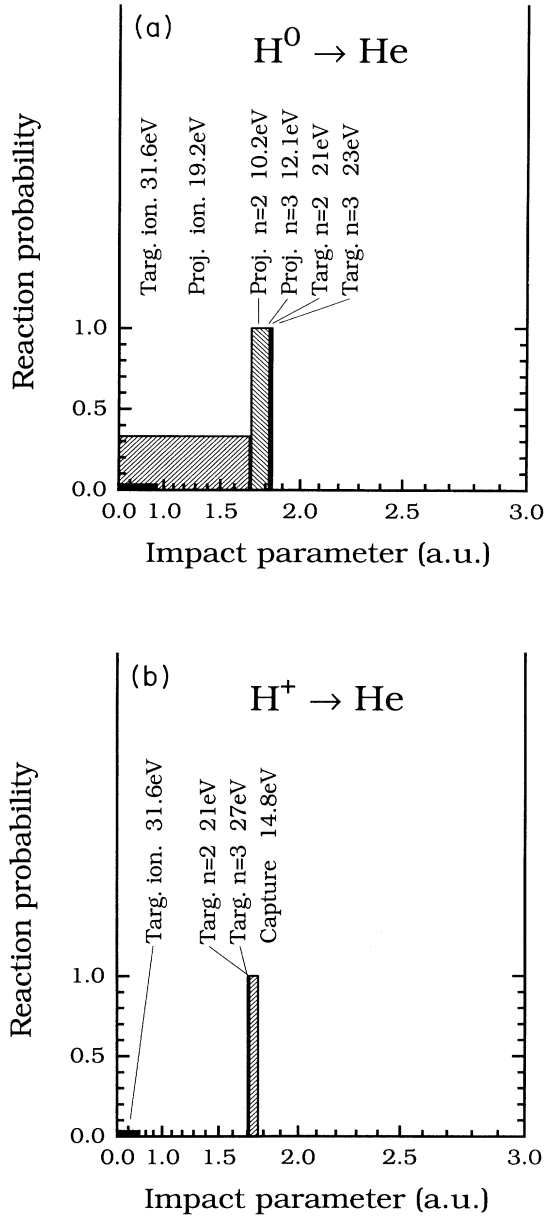

FIG. 8. Our model for the He atom with respect to the electronic energy loss of 8-keV hydrogen atoms (a) and protons (b). For abbreviations see Fig. 5.

D. Hydrogen

It was found by Phelps [1] that adding all available data on the individual energy-loss processes in hydrogen gas underestimates the measured ϵ by more than 30%. This can be seen also from Fig. 9, where our experimental data are shown; it covers all combinations of incident protons and deuterons onto H_2 and D_2. Also plotted in a *cumulative* manner are the contributions from charge-changing collisions and from energy-loss processes at fixed projectile charge state; no correction factor is applied to the cross sections. Looking at the experimental data we find only a very small dependence of ϵ on gas pressure and on projectile mass, well within the quoted experimental error.

The values of β that describe the velocity dependence of ϵ are $\beta=0.79$ at 4 keV (per nucleon), $\beta=0.62$ at 10 keV, and $\beta=0.50$ at 20 keV; contrary to the noble gases, β is smaller than 1. Even at 2 keV per nucleon, corresponding to $0.28v_0$, velocity proportionality does not hold.

E. Discussion

The question arises of whether the discrepancy found between the sum of the individual inelastic collisions and the measured ϵ (as expressed by the correction factor) may be explained by the errors of the underlying cross sections, or indicates that some energy-loss channels are missing. Unfortunately, most of the errors claimed for the relevant individual contributions are of the order of 30%, even for H_2 and He, where recommended cross sections [3] from an extensive compilation have been used for the most prominent collision processes; in particular, the data on processes induced by neutral hydrogen projectiles are rather inaccurate. For atomic targets (He, Ne) we find moderate differences over more than one order of magnitude in projectile energy. At least at some energy both results agree. So one could conclude that the discrepancies can be attributed to uncertainties in the cit-

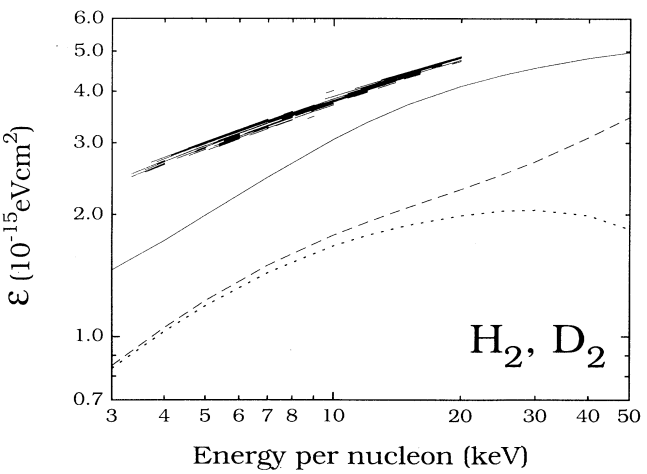

FIG. 9. Specific energy loss of protons and deuterons in H_2 and D_2. For details, see caption of Fig. 4.

ed cross sections. This does not apply to molecular targets (H_2, D_2) where the measured stopping cross sections are always substantially higher. It is very likely that dissociative processes might not have been fully accounted for [30]; in particular, no data for dissociation of excited molecules into unexcited neutral fractions seem to be available.

V. SUMMARY

We have measured the stopping cross sections of H_2, D_2, He, and Ne for hydrogen projectiles with energies between 3 and 20 keV per nucleon and have simulated our TOF experiment by a Monte Carlo program; in this way we can show the following two points.

(i) The assumption that the stopping cross section at low energies is proportional to projectile velocity ($\epsilon \propto v_1^{\beta}$, with $\beta = 1 = \text{const.}$) does not hold for these gases. Especially when the cross section for electron capture by the projectile is small (due to a large mismatch of the energy levels involved) an essential energy-loss mechanism at low velocities, i.e., by charge-changing processes, is impeded and β gets appreciably larger than 1 (this does not mean that charge changing may be ignored, cf. Fig. 7). But even when the capture cross section is large, β is only roughly equal to 1 and depends on velocity in this energy range.

We speculate that velocity proportionality, up to now considered strictly valid for metals, might not hold for those metals in which the effective density of the electron gas varies with projectile velocity (transition metals and noble metals) [31].

(ii) In transmission experiments at low velocities the impact-parameter-dependent *electronic* energy loss causes a noticeable influence of target thickness and of projectile mass on the measured specific energy loss; impact-parameter-dependent *nuclear* energy loss is too small to fully account for these effects. However, a detailed study of impact-parameter-dependent energy loss is not possible under conditions necessary in a stopping experiment because of the intrinsic inhomogeneity of gas targets at low pressures. From our measurement and simulation, one might deduce a residual influence of projectile mass on the electronic stopping cross section, that could be due to a Coulomb effect [29].

ACKNOWLEDGMENTS

The authors appreciate the hospitality of the Institut für Allgemeine Physik, Technische Universität Wien, where the experiments have been done. This project has been supported by the Fonds zur Förderung der wissenschaftlichen Forschung under Contract Nos. P6279-PHY and P8699-PHY.

[1] A. V. Phelps, J. Phys. Chem. Ref. Data **19**, 653 (1990); **20**, 1339 (1991).
[2] R. K. Janev, W. D. Langer, K. Evans, Jr., and D. E. Post, Jr., in *Elementary Processes in Hydrogen-Helium Plasmas,* edited by G. Ecker, Springer Series on Atoms and Plasmas, Vol. 4 (Springer, Berlin, 1987).
[3] C. F. Barnett, ORNL Publication No. ORNL-6086/V1 (Controlled Fusion Atomic Data Center, Oak Ridge National Laboratory, 1990) (unpublished).
[4] R. Golser and D. Semrad, Phys. Rev. Lett. **66**, 1831 (1991).
[5] R. Golser and D. Semrad, Phys. Rev. A **45**, 4222 (1992).
[6] D. Semrad and R. Golser, Nucl. Instrum. Methods Phys. Res. B **72**, 132 (1992).
[7] R. Ishiwari, N. Shiomi, T. Katayama-Kinoshita, and F. Sawada-Yasue, J. Phys. Soc. Jpn. **39**, 557 (1975); see also R. Ishiwari, N. Shiomi, and N. Sakamoto, Phys. Lett. **75A**, 112 (1979).
[8] R. Ishiwari, N. Shiomi-Tsuda, N. Sakamoto, and H. Ogawa, Nucl. Instrum. Methods Phys. Res. B **48**, 65 (1990).
[9] W. N. Lennard, Xia Yueyuan, and H. Geissel, Nucl. Instrum. Methods Phys. Res. B **69**, 89 (1992).
[10] L. Meyer, M. Klein, and R. Wedell, Phys. Status Solidi B **83**, 451 (1977).
[11] P. Mertens and Th. Krist, Nucl. Instrum. Methods Phys. Res. B **13**, 95 (1986).
[12] E. Clementi and R. Roetti, At. Data Nucl. Data Tables **14**, 177 (1974).
[13] H. H. Andersen, F. Besenbacher, P. Loftager, and W. Möller, Phys. Rev. A **21**, 1891 (1980).
[14] J. Lindhard, V. Nielsen, and M. Scharff, K. Dan. Vidensk. Selsk., Mat.-Fys. Medd. **36**, No. 10 (1968).
[15] P. L. Grande and G. Schiwietz, Phys. Rev. A **44**, 2984 (1991); Phys. Lett. A **163**, 439 (1992).
[16] N. M. Kabachnik, V. N. Kondratev, and O. V. Chumanova, Phys. Status Solidi B **145**, 103 (1988).
[17] H. H. Mikkelsen and P. Sigmund, Nucl. Instrum. Methods Phys. Res. B **27**, 266 (1987).
[18] H. H. Mikkelsen and H. Flyvbjerg, Phys. Rev. A **45**, 3025 (1992).
[19] W. Fritsch and C. D. Lin, Phys. Rep. **202**, 1 (1991).
[20] N. M. Kabachnik, Nucl. Instrum. Methods Phys. Res. B **69**, 76 (1992).
[21] A. D. Marwick and P. Sigmund, Nucl. Instrum. Methods Phys. Res. **126**, 317 (1975).
[22] P. Sigmund and K. B. Winterbon, Nucl. Instrum. Methods Phys. Res. **119**, 541 (1974).
[23] H. Tawara, At. Data Nucl. Data Tables **22**, 491 (1978).
[24] R. H. Hughes, H. M. Petefish, and H. Kisner, Phys. Rev. A **5**, 2103 (1972).
[25] E. W. Thomas, *Excitation in Heavy Particle Collisions* (Wiley, New York, 1972), p. 171.
[26] Wen-qin Cheng, M. E. Rudd, and Ying-Yuan Hsu, Phys. Rev. A **39**, 2359 (1989).
[27] R. J. McNeal, D. C. Clark, and R. A. Klingberg, Phys. Rev. A **2**, 131 (1970).
[28] M. E. Rudd, Y.-K. Kim, D. H. Madison, and T. J. Gay, Rev. Mod. Phys. **64**, 441 (1992).
[29] D. Semrad, Phys. Rev. A **33**, 1646 (1986).
[30] M. Inokuti (private communication).
[31] D. Semrad and R. Golser, Phys. Rev. A **35**, 4836 (1987).